Optical cavity spectroscopy using heterodyne detection with optical feedback laser frequency locking

Marianne Beaumont, Irène Ventrillard, Daniele Romanini

Optical cavity spectroscopy using heterodyne detection with optical feedback laser frequency locking

MARIANNE BEAUMONT[1], IRÈNE VENTRILLARD,[1] AND DANIELE ROMANINI [1,*]

[1] *Univ. Grenoble Alpes, CNRS, LIPhy, F-38000 Grenoble, France*
[*] *daniel.romanini@univ-grenoble-alpes.fr*

Abstract: We demonstrate an accurate high sensitivity method for cavity spectroscopy. We measure the frequency intervals of transverse electromagnetic modes relative to a fundamental mode in a high finesse optical resonator, and attribute their mode numbers unambiguously. A laser is frequency locked to a fundamental TEM_{00} cavity mode by optical feedback, and phase modulation is used to obtain frequency side bands, which may come to resonance with other transverse cavity modes as the radio-frequency of the modulation is tuned. At these resonances, transmission of the side bands is sensitively detected by heterodyning with the carrier. We also analyse the transverse spatial profile of the heterodyne signal for identification of mode numbers. The adjustment of the Gaussian cavity model to the measured frequency intervals yields accurate values of cavity length, mirrors radius of curvature and mirrors ellipticity, to the ppm level.

1. Introduction

Optical resonant cavities are widely used in different domains of optics, such as interferometry [1], spectroscopy [2], or time-frequency metrology [3, 4], since their properties are useful to increase sensitivity and/or spectral resolution. In particular, frequency locking of a laser to a cavity resonance is an effective means to stabilize its emission frequency and reduce its emission linewidth [5]. Among other means, optical feedback (OF) may be put to profit for this, especially for distributed feedback (DFB) laser diodes [6]. OF fast and efficient locking of a semiconductor laser to an optical cavity has been exploited to perform absorption spectroscopy of gas samples with high sensitivity for trace analysis applications [7, 8]. It was also exploited to obtain other types of sensitive measurements in optics such as birefringence effect [9] or polarisation mode splitting [10].

For some applications, consideration of the transverse modes may be of importance because their frequency splitting and probability of injection depend on the geometry of the cavity and on the alignment and focussing of the input beam, respectively. Heterodyne detection of transverse modes was especially exploited in gravitational interferometers, as a probe of the correct alignment [1, 11] and to verify the geometrical parameters of the cavity, such as mirror separation and curvature radius, as well as to reveal the presence of astigmatism due to mirror deformation [12].

In this work, we demonstrate accurate measurements of the frequency separation of the transverse electromagnetic (TEM_{mn}) resonances of a high finesse optical cavity with a technique relying on OF frequency locking and heterodyne detection. A diode laser is frequency locked to a TEM_{00} cavity mode, and we use phase modulation to obtain frequency side bands, which may come to resonance with other transverse cavity modes as the radio-frequency (RF) of the modulation is tuned. In order to observe the occurrence of these resonances we use heterodyne detection. In other words, we detect the RF beating signal between the laser locking mode and the injected side band at cavity transmission by using a fast photodiode. Specifically, the laser-cavity frequency locking is obtained by optical feedback (as done in [10]), but other locking schemes have been used, such as the well-known Pound-Drever-Hall method [5], in other approaching

setups [1, 11, 12]. It should be noted that OF locking is particularly adapted to a V-shaped cavity geometry, but it can also be implemented with linear cavities [9, 13, 14]. Moreover, contrary to the Pound-Drever-Hall method, OF locking works well with semiconductor lasers possessing high phase noise and correspondingly large linewidth. Indeed, OF locking induces a spectacular narrowing in DFB diode lasers emission, to below the resonator line width [6, 15, 16].

Comparison of the beat note measurements with a model allows to retrieve the length of the cavity down to a few microns accuracy, and the mean radius of curvature of the mirrors down to ten microns accuracy along orthogonal transverse directions, allowing to assess mirrors ellipticity. These parameters are deduced after identification of the transverse indices m and n of the resonances, from intensity measurement of the transverse mode profiles. Frequency deviation from the fundamental TEM_{00} mode and spectral widths of the resonances are also accurately measured, allowing assessment of the surface homogeneity of mirror losses.

2. Experimental setup

Our experimental setup is outlined in fig. 1. A distributed feedback diode laser (DFB), emitting at 1.65 μm, is optically locked to a fundamental transverse TEM_{00} mode of a V-shaped cavity. The optical feedback from the optical cavity induces strong laser line-width narrowing, delivers intense and steady cavity transmission signal, and locks the diode laser frequency to the TEM_{00} mode [6, 16]. A detailed description and discussion of this type of OF locking setup can be found e.g. in [17]. This section will provide specific modifications from the standard setup, implemented in this work for the cavity spectroscopy by heterodyne detection.

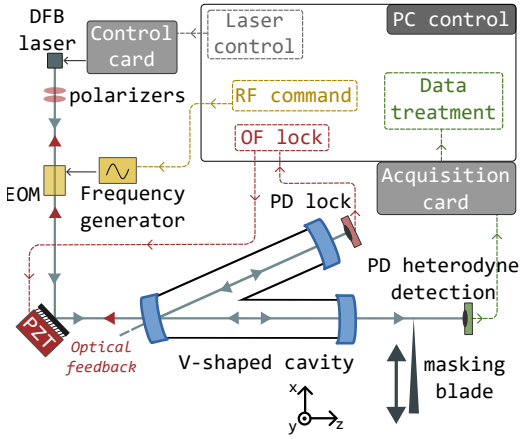

Fig. 1. Diagram of the experimental setup. The optical cavity (in blue) is a V shaped cavity made of 3 identical mirrors, with an arm length of roughly 49 cm and a small angle of incidence at the folding mirror of 0.44°. Mirror radius of curvature is specified to 100 cm. The laser is locked to a TEM_{00} mode by detection of the transmitted signal ("PD lock") and by phase control of the optical feedback (OF) acting on a piezoelectric (PZT) mounted mirror. An electro-optic modulator (EOM) allows to create side bands at a radio-frequency (RF) digitally controlled. A second photodiode monitors the RF heterodyne signal. A masking blade, mounted in a translation stage, allows to cut off part of the cavity output beam before heterodyne detection.

The OF rate is controlled by an attenuator composed here of two successive polarisers, the second one having a fixed orientation in the plane of the V-cavity (x-axis in fig. 1). The OF phase is controlled to a fraction of a wavelength by acting on a PZT-mounted mirror before the cavity [17]. A photodiode (100 kHz bandpass) monitoring one of the two cavity outputs delivers

the cavity transmission signal used for OF phase control. In the present implementation, the error signal for OF phase stabilization is obtained by frequency scanning the laser diode across a single TEM_{00} cavity mode at a repetition rate of 10 Hz in order to derive the asymmetry of the mode profile. This allows to obtain heterodyne signal during the few ms when the laser is locked to the center of the resonance.

The laser beam is phase modulated with an EOM (electro-optic modulator) in order to create frequency side bands. The EOM extraordinary axis is aligned with the beam polarisation in order to create pure phase modulation and insignificant beam ellipticity. The beam polarisation is chosen to be in the plane of the cavity (x-axis) to ensure that only horizontal polarisation cavity modes are excited thus avoiding complications associated with polarization modes and their splitting in such a cavity (due to off normal reflection on the folding mirror). The EOM is fed with a sine signal produced by a RF synthesizer (Rohde&Schwarz SMB100A) digitally controlled. We keep a low power on the side bands compared to the carrier (about 1 %), thus no RF amplifier is needed. This is largely sufficient to obtain strong heterodyne signals. As the RF modulation is swept, one or the other of the side bands can resonate with transverse cavity modes (TEM_{mn}) and be transmitted by the cavity together with the carrier which is always present due to the OF locking. To increase the injection of different transverse modes, the beam is not perfectly mode-matched to the cavity. One should note that OF locking to the TEM_{00} mode is sufficiently robust to tolerate higher side band levels (up to several percent), and that even with a non optimal mode matching.

The optical V-cavity is made of three mirrors coming from the same batch, spaced by about 49 cm (fig. 1), with radius of curvatures specified to 1 m. This means we are close to a half-confocal configuration (which would correspond to cavity length of 50 cm), with transverse modes frequencies falling roughly at one-third (for the modes with $m + n = 1$) and two-thirds (modes with $m + n = 2$) of the cavity Free Spectral Range (FSR, which is about 150 MHz) [18]. Hence, to inject TEM_{mn} modes while the laser is locked to a TEM_{00} mode, it is sufficient to sweep the RF frequency of a few MHz around 50 MHz. The modes whose frequencies are around $FSR/3$ are injected by the upper side band, while the lower side band injects modes whose frequencies are around $2FSR/3$.

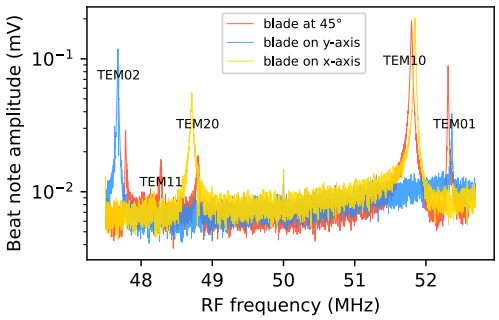

Fig. 2. Beat note amplitude at cavity output, between a side band and the carrier, as a function of the modulation frequency (RF). Measurements recorded on different days and for different blade angles used to mask part the cavity output beam and produce heterodyne signals (see text).

As the RF is swept, the beat note is recorded on a high bandwidth photodiode placed at the second cavity output ("heterodyne PD" in fig. 1, 150 MHz bandwidth). Its signal is sampled by a high speed acquisition card (Gage Razor Compuscope, 200 MHz acquisition frequency) installed in a personal computer. Fourier transform is then computed to obtain the beat note amplitude at

the RF frequency. A Labview software allows to control the RF frequency and to perform data acquisition and processing in order to record the frequency profiles of the transverse mode as a function of the RF frequency (fig. 2). The transverse mode spectral width and frequency interval from the TEM_{00} can then be accurately determined by a Lorentzian fit.

In fig. 2, transmission spectra of five detected transverse modes are shown, whose frequencies fall around 50 MHz from the TEM_{00} mode as expected. The small divergence of our setup from the half-confocal configuration is enough to ensure that both side bands are not injected in the cavity at once, as the frequencies of the groups of modes differ of a few MHz from $FSR/3$ and $2FSR/3$. Furthermore, because of mirrors ellipticity, modes of same order $m + n$ are not degenerated. Their frequency separation (~ 0.5 MHz) is much larger than their spectral width (~ 20 kHz), therefore only one side band is transmitted at a time and allows to detect individually each mode.

It is interesting to note that the heterodyne signal is different from zero only when a side band is transmitted, contrary to normal transmission measurement. Such zero background measurement is then not affected by source amplitude fluctuations which would degrade the sensitivity. In addition, even though the side band has low power and is additionally poorly coupled to the cavity transverse modes (given the non optimal mode-matching), heterodyne detection provides an important optical amplification effect before detection. This is due to the beat signal being the product of the side band field with the strong carrier field. The noise level of our measurement (fig. 2) is estimated to correspond to a side band detection limit of 60 fW. Detected side band power levels range from 1 pW to 90 pW, while the carrier power at cavity output is 8 µW. This was obtained with acquisition at 200 Msamples/s, acquired during 2.6 ms, leading to a Fourier resolution of 380 Hz. Side bands have been detected with a power ratio at cavity output with the carrier of around 10^{-6}.

Mode frequencies are seen to shift (up to 100 kHz) from one acquisition to the other because the three sets of data in fig. 2 have been recorded at several days of interval. Indeed, the cavity is not thermally regulated. If direct impact of thermal cavity length change on mode frequencies is negligible for room temperature of 1 °C, mode separation is very sensitive to changes of the mirrors surface curvature (also affected by drifting mechanical stress). We see from the model (introduced in the following) that a change of 0.15 % on the radius of curvature of the mirrors shifts the transverse modes by more than 100 kHz.

The last key element in the setup is the masking blade placed before the heterodyne photodiode (fig. 1), that allows to partially cut the transmitted beam. This is necessary as the TEM cavity modes form a basis of orthogonal functions [19], thus the unbounded overlap integral of any two modes of different orders m, n is null when taken over any transverse surface.

This spatial orthogonality must be removed in order to observe a beat note when a side band is resonant with a transverse mode. Various methods have been previously used. For example, Mueller et al. [11] used a ring-segment photodiode whose individual segments are smaller than the transverse extent of the beam, resulting in a non-zero signal for each segment. Here, we proceed by partially masking the output beam from the cavity (as Stochino et al. [12]), using an opaque blade placed in front of the heterodyne detection photodiode (fig. 1). As shown in fig. 2 and as discussed in section 4, according to the angle of the edge of the blade in the (xy) plane some modes are detected or not. The blade is mounted on a motorized translation stage in order to study the beat note amplitude as a function of the masked area. However, if the beam is not perfectly focussed on the photodiode, then it is partially cut and the beat note is non null even without using the masking blade. To ensure to have a zero background, we adjusted the alignment of the beam on the photodiode to have a zero beat note with the full beam. This is further discussed in section 4.

3. Transverse modes frequencies analysis

The frequencies of TEM_{mn} modes are computed using the standard ABCD matrices formalism for Gaussian beam propagation to describe the beam path in the cavity as a single round-trip matrix ([19], chap.7.2). Then, the recursive condition ([19], eq. 7.3-1) on the complex phase of the beam allows to find the resonant frequencies. The cavity round-trip matrix contains a reduced number of effective parameters (curvature radii, cavity angle and cavity length) on which the transverse mode frequencies depend. To account for ellipticity, two round-trip matrices are computed, one on each transverse axis x and y. The effect of the non-zero angle of incidence at the folding mirror (θ) and mirror ellipticity cumulate, as the angle of reflection on the folding mirror are equivalent to a modification of the radius of curvature of $\cos(\theta)$ in the horizontal plane and $1/\cos(\theta)$ in the vertical plane. We then fixed the angle to $\theta = 0.44°$ (deduced from the mechanical design), so that the ellipticity calculated below is intrinsic to the mirrors.

It is interesting to note that we can adopt the simplifying assumption that the 3 cavity mirrors are identical, with the same radius of curvature (R_x in the horizontal and R_y in the vertical directions). Actually, each mirror of a cavity is certainly affected by specific distortions of the curvature radius in any transverse direction, due to manufacturing imprecision and mounting mechanical stress. However, if we can consider these distortions as small perturbations relative to the radius specified by the manufacturer, we can show that, at the first order, the round-trip Gaussian propagation matrix for each transverse direction can be rewritten with all the mirror radii being fixed at the nominal value modified by only one and the same perturbation parameter. A proof of this is given in the Appendix. In the case of mirrors with the same specifications as in our setup, we can use just two adjustable parameters for the perturbed radii in the x and y directions. We will then have to confirm that the difference of the values giving the best match of the experimental resonance frequencies are actually close to the nominal radius given by the manufacturer.

We then adjusted the values of the mean radii of the mirrors on axes x and y, and the value of the cavity length, so that the calculated frequencies of the transverse modes correspond as closely as possible to the measured frequencies. This was achieved by manual adjustment without setting up a specific fitting routine, although for future experiments using this configuration, this should achieve better accuracy and precision for the cavity parameters, and be much more effective in the case of a repeatable and systematic study.

The comparison between the calculated frequencies and the measured ones is presented in table 1. We reached a good agreement, to less than 10 kHz, which is smaller than the day to day variability of the measurements (long term drifts can lead to differences of over 100 kHz, as seen in fig. 2). Experimental accuracy is limited by the temporal resolution of the acquisition and the SNR of the mode detection, and is therefore improved for more strongly injected modes. For all modes, accuracy is under the kHz, well below the spectral width of the transverse modes (about 20 kHz).

Model fitting gives a cavity arm length of 49.1910 cm ± 5 µm (corresponding to an FSR of 152.3924 MHz). This value is consistent with macroscopic measurements, but is far more accurate than any dimensional metrology. The mean radius of curvature of the mirrors obtained from the model is 100.6096 cm ± 10 µm, and the ellipticity (difference between the radius of curvature on the x-axis and the y-axis) is 0.9180 cm ± 3 µm. This is within the manufacturer's specifications (1 m with 1 % accuracy), but the ellipticity is quite large, close to 1 % of the mirror curvature. Uncertainties on cavity parameters are estimated by modifying each parameter independently until the difference of all calculated mode frequencies diverges by more than 10^{-3}. This method does not take into account the correlation between the various parameters. This method hence yields values at the ppm level for our setup.

We were able to detect 5 transverse modes. The injection of these modes depends on mode matching, offset and angle relative to the cavity propagation axis [20]. The injection of other

mode	model (MHz)	experiment (MHz)	difference (kHz)	mode width
TEM_{02}	47.7829	47.7831(2)	−0.2	12.9 kHz
TEM_{11}	48.2880	48.2785(4)	9.5	23.0 kHz
TEM_{20}	48.7931	48.7974(4)	−4.3	34.7 kHz
TEM_{10}	−51.7997	−51.79831(3)	1.4	19.1 kHz
TEM_{01}	−52.3048	−52.31202(2)	−7.2	10.1 kHz

Table 1. Transverse mode frequencies relative to the TEM_{00} mode, obtained by adjustment of the model to fit experimental values derived from the measurements plotted in red in fig. 2. The given width is full width at half maximum of the measured beat note.

modes would then be possible by modifying the beam alignment. In our case, we used the 5 detected modes to deduce the cavity parameters. This would be possible with a minimum of one mode on each transverse axis, although with fewer modes the accuracy would be degraded. On the other hand, if more modes can be detected, accuracy will be improved, enabling the model to be constrained more effectively.

The heterodyne beat note acquisition shown in fig. 2 allows to measure directly the spectral width of the transverse modes. Indeed, the laser carrier frequency being locked by optical feedback to the TEM_{00} mode, its spectral width falls far below the width of the TEM_{00} mode [6, 15, 16]. In addition, the locked frequency is stabilized to the centre of the TEM_{00} mode to a small fraction of the mode linewidth. Hence the side band is then a direct probe to the width of the transverse mode. In addition, the cavity is flushed with dry nitrogen to prevent any absorption loss by molecular absorption lines. This insures that the observed spectral widths correspond to the intrinsic cavity losses for each transverse mode. The values of the full width at half maximum (FWHM) are given in table 1. The FWHM of TEM_{00} mode can be deduced from the measurement of the cavity ring-down time thanks to the following relation ([8], eq.1.3, modified to account for a V cavity):

$$\tau_{rd} = \frac{1}{2\pi\Delta\nu} = \frac{L}{2c}\frac{\sqrt{\mathcal{R}}}{1-\mathcal{R}} \tag{1}$$

where τ_{rd} is the ring-down time of the mode, $\Delta\nu$ is the mode width, L is the total cavity length (here $2 * 49.191$ cm), R is the reflectivity of the mirrors and c the speed of light. We can see that the ring-down time and the mode width are both related to the cavity losses through the reflectivity coefficient R. The measured ring-down time for TEM00 mode is $\tau_{rd} = 11.0$ µs, corresponding to a finesse $F \sim 10570$, and a mode width of 14.5 kHz. The measured FWHM of transverse modes are then in the same range as the TEM_{00}'s FWHM.

However it must be noted that the actual transverse mode widths are different and vary as seen in table 1 from 10.1 to 34.7 kHz, respectively for the TEM_{01} and TEM_{20} modes.

These differences can be explained by the transverse spatial distribution of the field on the mirrors, which is specific to each transverse mode. Indeed, if the mirrors have defects that lie within the spatial lobes of a mode, the effective reflectivity of the mirror will be modified for that mode and, consequently, the width of that mode (see equation τ_{rd}). In our case, we can hypothesize that there is a defect on a mirror that falls on the x-axis, as TEM modes along the x-axis have wider FWHMs than others. Although we have not investigated this aspect further, it is clear that the spectral width of transverse modes can be useful for characterizing mirror defects.

4. Transverse modes spatial profile

As TEM_{mn} modes are all orthogonal to each other, the product of the fields of a TEM_{00} and of a TEM_{mn} mode, when integrated over the PD transverse plane, must yield a zero beat note. This is true for any transverse mode, and not just for antisymmetric modes, unlike what seems to be asserted in [12].

When the RF frequency matches the separation of a TEM_{mn} mode from the TEM_{00} laser lock mode, the beat note amplitude between this mode and the TEM_{00} depends on the position of the edge of the masking blade relative to the beam centre and on its angle relative to the transverse x, y axes. We have made measurements with the edge of the blade along the x-axis moving it vertically, with the edge on the y-axis moving it horizontally, and at an angle of 45°. In the following, when we will say that the blade is along a given axis, we will mean that its edge is along that axis. It should be noted that transverse modes were not initially along the principal axes of the setup: they had an angle of more than 30° with the plane of the cavity. The orientation of transverse mode profiles depends on the ellipticity of the optical system [21]. The fact that it is not along the principal axes implies that mirrors ellipticities have a stronger effect than the ellipticity induced by the cavity angle. For convenience, we made sure that the transverse mode profiles are aligned with the principal axes x and y of the cavity. To do this, we locked the laser on transverse modes by slightly degrading injection alignment and reducing OF, in order to monitor the transmitted beam on a camera. Then we adjusted cavity mirror mounts stress to reduce mirror ellipticity until observing modes aligned along the principal axes.

The expected beat note dependence on position and blade angle can be calculated as the product between the two modes integrated over the region of transverse space that is not masked by the blade and therefore produces a signal on the photodiode. We express this as follows : I_{beat} is the beat note amplitude, E_{00} and E_{mn} are the modes fields (the full expression of the modes is found in [2], eq.1), and they depend on the frequency ν, the blade edge position in the transverse plane D (with origin at the beam centre), and on the position of the blade translation plane along the propagation axis z, while the angle of the blade is expressed by different parametrization of the integration limits:

$$x\text{-axis} : I_{beat,mn}(D,\nu,z) = 2 \cdot \left| \int_{D}^{\infty} \int_{-\infty}^{\infty} \overline{E_{00}(\nu,x,y,z)} \cdot E_{mn}(\nu,x,y,z)\, dy\, dx \right| \tag{2}$$

$$y\text{-axis} : I_{beat,mn}(D,\nu,z) = 2 \cdot \left| \int_{-\infty}^{\infty} \int_{D}^{\infty} \overline{E_{00}(\nu,x,y,z)} \cdot E_{mn}(\nu,x,y,z)\, dy\, dx \right| \tag{3}$$

$$45° : I_{beat,mn}(D,\nu,z) = 2 \cdot \left| \int_{-\infty}^{\infty} \int_{x-D}^{\infty} \overline{E_{00}(\nu,x,y,z)} \cdot E_{mn}(\nu,x,y,z)\, dy\, dx \right| \tag{4}$$

From these integrals, it is possible to choose the optimum blade position to obtain the maximum signal when scanning the RF side band. Simulated beat traces are shown in fig. 3 for three transverse modes TEM_{01}, TEM_{02} and TEM_{11}, each beating with a TEM_{00} mode. The beat notes obtained with modes of order $m+n=2$ (TEM_{02} and TEM_{11}) show a characteristic double hump, while the TEM_{01} mode shows only a single maximum. The characteristic mode shapes result from the presence of Hermite polynomials in the definition of Hermite-Gauss modes. The effect of the blade angle allows the direction of the transverse mode to be identified: for example, the TEM_{02} mode gives a null profile for the beat note when the blade is along the x axis, while it gives a non-zero profile when the blade is along the y axis, and the opposite is obtained for the TEM_{20} mode. On the other hand, the TEM_{11} mode gives null beat note profiles when the blade edge is along both axes, and the blade must be tilted, for instance at 45°, for the beat note to become visible.

In fig. 4, we show the beat note recorded at a fixed RF frequency (corresponding to the RF peak of each transverse mode), as a function of the position of the blade. This was done with the

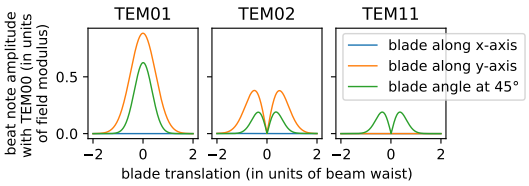

Fig. 3. Expected amplitude of the beat note with TEM_{00} field, for several TEM_{mn} modes, according to the position of the edge of the masking blade in the transverse plane, and for different blade angles. The beam waist corresponds to the transverse radius of the beam at the position of the blade along the propagation axis.

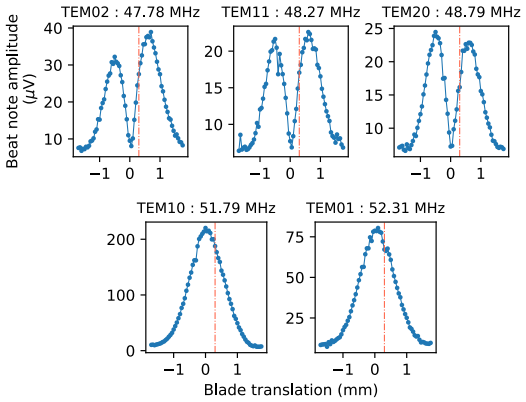

Fig. 4. Measured beat note amplitude of transverse modes according to the masking blade position. The blade angle is 45°. For each mode, this is recorded at a fixed modulation frequency corresponding to the resonant frequency of their respective transverse modes. The red dashed lines show the position of the blade during acquisition of the data presented in fig. 2, blade at 45° in red line.

blade at a 45° angle, in order to record all the modes at once. The red dashed lines indicate the position of the blade for the red trace in fig. 2 : this highlights the fact that to see all 5 modes, the blade must also be positioned out of the beam centre, otherwise modes such as $m + n = 2$ are undetectable. Double humps can be seen for the triplet of $m + n = 2$ modes and a single hump for the doublet of $m + n = 1$ modes. We did the same with the blade along the x and y axes, we found as expected that some modes are not visible, allowing us to assign the indices m and n to the corresponding modes without any possible confusion. The extinction can be seen in fig. 2, where when the blade is along the x-axis (yellow line) we see only the TEM_{20} and TEM_{10} modes, when it is along the y-axis (blue line) we see only the TEM_{02} and TEM_{01} modes, and for the blade at 45° (red line) we see all five modes.

If transverse modes of higher order are injected in the cavity (depending on cavity parameters and mode matching), the use of a masking blade will work all the same to identify their indices m and n.

5. Conclusion

In this work we demonstrate high precision cavity spectroscopy by combining optical feedback locking of a laser diode to a cavity mode, with heterodyne detection at cavity transmission after imposing frequency side bands to the laser. Optical heterodyne detection requires to remove

mode orthogonality by partially masking the transmitted beam before detection. When scanning the side band frequency, the heterodyne amplitude provides transverse mode excitation spectra relative to the locked cavity mode with high sensitivity and a zero background. This yields the relative frequencies of transverse modes even if they are weakly injected. Moreover, while keeping one side band resonant with a transverse mode, scanning the blade position yields transverse intensity profiles corresponding to the spatial profile of that mode, allowing direct identification of its transverse order. The frequency measurements that we obtain are then used to adjust a cavity model that yields the geometrical cavity parameters with high precision (on the ppm levels in our case). The relative amplitude of the heterodyne signal according to the modes is not studied further in this work, but it could be used to obtain information about the injection coefficients of transverse modes, which depend on the alignment and mode matching [20].

Finally, the spectral width of transverse modes is also accurately measured, which correspond directly to cavity losses. We have observed that the spectral widths are quite different according to the transverse mode. This clearly implies that our mirrors have non uniform surface quality (assuming our cleaning procedure removed all impurities). Measurements of the width of even more transverse modes with higher orders should in principle allow to build a map of surface losses.

While other laser locking techniques can be used, optical feedback was found to provide robust and reproducible results and to work well with standard DFB lasers in the near infrared region.

In our setup, monitoring transverse mode frequencies is quite slow (a few minutes to scan 5 MHz and infer the frequencies) as it requires to sweep the RF frequency between each acquisition.The acquisition time can be significantly reduced with consistent experimental modification, for example with several single RF modulations corresponding to transverse mode frequencies able to inject all transverse modes at once.

Our method allows to detect side band power down to fW levels even with a small carrier power transmitted through the cavity (0.4 ‰ of the laser beam initial power). Increasing the power of the carrier may lead to detection of even lower side bands, but this must be done without increasing the OF. This is possible by replacing the 2 polarisers (which attenuate the beam in both directions) by an adjustable optical isolator, as it would allow the full laser power to be delivered to the cavity, with only a small fraction coming back for OF.

6. Appendix

We are going here to demonstrate that in the limit of small deformations of the mirrors surfaces, one can use a single distortion parameter for each cavity transverse axis x and y to account for the deformations of all mirrors composing an optical cavity. This is valid independently of the shape of the cavity (linear, V shaped, bow tie, ring ...). The first hypothesis is that the cavity admits two orthogonal axes, thus being well described by Hermite-Gauss modes relative to orthogonal x and y transverse axes. In this case, one can write a round-trip Gaussian propagation matrix for each axis.

We start by considering that each of the 3 mirrors (identified in the following by an integer m) is affected by different perturbations of the curvature in each transverse direction, due to manufacturing imprecision and mounting mechanical stress. The matrix for cavity mirror m along x (to fix things) will then be :

$$M_m = \begin{pmatrix} 1 & 0 \\ -\frac{2}{R_m+\epsilon_m} & 1 \end{pmatrix} \tag{5}$$

where $\epsilon_m << R_m$ is the small deformation parameter for the mirror curvature radius R_m along x (this would be the value given by the manufacturer). The mirror matrix for Gaussian beam propagation along x will be the ordered chain product of this matrix with propagation matrices for

the free space in between cavity mirrors and similar matrices as eq. (5) for other cavity mirrors, each with a given curvature radius and deformation parameter. For example for a V shaped cavity (of equal arms of length d) this round trip matrix will be :

$$M = \begin{pmatrix} 1 & d \\ 0 & 1 \end{pmatrix} \cdot \begin{pmatrix} 1 & 0 \\ -\frac{2}{R_2+\epsilon_2} & 1 \end{pmatrix} \cdot \begin{pmatrix} 1 & d \\ 0 & 1 \end{pmatrix} \cdot \begin{pmatrix} 1 & 0 \\ -\frac{2}{R_3+\epsilon_3} & 1 \end{pmatrix} \cdot \begin{pmatrix} 1 & d \\ 0 & 1 \end{pmatrix} \cdot \begin{pmatrix} 1 & 0 \\ -\frac{2}{R_2+\epsilon_2} & 1 \end{pmatrix} \cdot \begin{pmatrix} 1 & d \\ 0 & 1 \end{pmatrix} \cdot \begin{pmatrix} 1 & 0 \\ -\frac{2}{R_1+\epsilon_1} & 1 \end{pmatrix} \tag{6}$$

We then recognize that the perturbed mirror matrix can be written, at the first order in ϵ/R as the product of the unperturbed matrix times a perturbation matrix, as follows :

$$M_m = \begin{pmatrix} 1 & 0 \\ -\frac{2}{R_m+\epsilon_m} & 1 \end{pmatrix} \approx \begin{pmatrix} 1 & 0 \\ -\frac{2}{R_m} & 1 \end{pmatrix} \cdot \begin{pmatrix} 1 & 0 \\ \frac{2\epsilon_m}{R_m^2} & 1 \end{pmatrix} \tag{7}$$

and it is easy to check that these two matrices commute. In addition, we can consider that the perturbation matrix commutes with the free space propagation matrix :

$$\begin{pmatrix} 1 & d \\ 0 & 1 \end{pmatrix} \cdot \begin{pmatrix} 1 & 0 \\ \frac{2\epsilon_m}{R_m^2} & 1 \end{pmatrix} = \begin{pmatrix} 1+\frac{d\cdot 2\epsilon_m}{R_m^2} & d \\ \frac{2\epsilon_m}{R_m^2} & 1 \end{pmatrix} \approx \begin{pmatrix} 1 & d \\ \frac{2\epsilon_m}{R_m^2} & 1 \end{pmatrix} \tag{8}$$

$$\begin{pmatrix} 1 & 0 \\ \frac{2\epsilon_m}{R_m^2} & 1 \end{pmatrix} \cdot \begin{pmatrix} 1 & d \\ 0 & 1 \end{pmatrix} = \begin{pmatrix} 1 & d \\ \frac{2\epsilon_m}{R_m^2} & 1+\frac{d\cdot 2\epsilon_m}{R_m^2} \end{pmatrix} \approx \begin{pmatrix} 1 & d \\ \frac{2\epsilon_m}{R_m^2} & 1 \end{pmatrix} \tag{9}$$

$$\text{hence} \quad \begin{pmatrix} 1 & d \\ 0 & 1 \end{pmatrix} \cdot \begin{pmatrix} 1 & 0 \\ \frac{2\epsilon_m}{R_m^2} & 1 \end{pmatrix} \approx \begin{pmatrix} 1 & 0 \\ \frac{2\epsilon_m}{R_m^2} & 1 \end{pmatrix} \cdot \begin{pmatrix} 1 & d \\ 0 & 1 \end{pmatrix} \tag{10}$$

where in the diagonal elements on the resultant matrix, the term $\frac{d\cdot 2\epsilon}{R^2}$ was neglected as compared to 1 (first order in ϵ/R and also because in general as $d/R < 1$ imposed by the cavity stability condition).

Thanks to these matrix commutation approximations, the perturbation matrices for all the mirrors composing the cavity can be displaced inside the round-trip matrix chain product and can be moved close together. Their product can be rewritten as a product of the same number of identical perturbation matrices :

$$\prod_{m=1}^{N} \begin{pmatrix} 1 & 0 \\ \frac{2\epsilon_m}{R_m^2} & 1 \end{pmatrix} = \begin{pmatrix} 1 & 0 \\ \sum_{m=1}^{N} \frac{2\epsilon_m}{R_m^2} & 1 \end{pmatrix} = \begin{pmatrix} 1 & 0 \\ N\cdot\alpha & 1 \end{pmatrix} = \prod_{m=1}^{N} \begin{pmatrix} 1 & 0 \\ \alpha & 1 \end{pmatrix} \tag{11}$$

where we introduce the global perturbation parameter $\alpha << R_m$ (for all m) given by the sum of $2\epsilon_m/R_m^2$ over the number of cavity mirrors N. These perturbation matrices can be replaced back together with the mirror matrices which now result to be affected by the same perturbation parameter.

Disclosures. The authors declare no conflicts of interest.

Data Availability Statement. Data underlying the results presented in this paper are not publicly available at this time but may be obtained from the authors upon reasonable request.

References

1. F. Magaña-Sandoval, T. Vo, D. Vander-Hyde, *et al.*, "Sensing optical cavity mismatch with a mode-converter and quadrant photodiode," Phys. Rev. D **100**, 102001 (2019).
2. D. Romanini, I. Ventrillard, G. Méjean, *et al.*, "Introduction to Cavity Enhanced Absorption Spectroscopy," Springer Ser. Opt. Sci. **179**, 1–60 (2014).
3. B. Dahmani, L. Hollberg, and R. Drullinger, "Frequency stabilization of semiconductor lasers by resonant optical feedback," Opt. Lett. **12**, 876 (1987).
4. S. Häfner, S. Falke, C. Grebing, *et al.*, "8×10^{-17} fractional laser frequency instability with a long room-temperature cavity," Opt. Lett. **40**, 2112 (2015).
5. R. W. P. Drever, J. L. Hall, F. V. Kowalski, *et al.*, "Laser phase and frequency stabilization using an optical resonator," Appl. Phys. B Photophysics Laser Chem. **31**, 97–105 (1983).
6. P. Laurent, A. Clairon, and C. Breant, "Frequency noise analysis of optically self-locked diode lasers," IEEE J. Quantum Electron. **25**, 1131–1142 (1989).
7. L. Richard, D. Romanini, and I. Ventrillard, "Nitric Oxide Analysis Down to ppt Levels by Optical-Feedback Cavity-Enhanced Absorption Spectroscopy," Sensors **18**, 1997 (2018).
8. J. Morville, D. Romanini, and E. Kerstel, "Cavity Enhanced Absorption Spectroscopy with Optical Feedback," in *Cavity-Enhanced Spectroscopy and Sensing,* vol. 179 G. Gagliardi and H.-P. Loock, eds. (Springer Berlin Heidelberg, Berlin, Heidelberg, 2014), pp. 163–209. Series Title: Springer Series in Optical Sciences.
9. M. Durand, J. Morville, and D. Romanini, "Shot-noise-limited measurement of sub–parts-per-trillion birefringence phase shift in a high-finesse cavity," Phys. Rev. A **82**, 031803 (2010).
10. L. Djevahirdjian, G. Méjean, and D. Romanini, "Gouy phase shift measurement in a high-finesse cavity by optical feedback frequency locking," Meas. Sci. Technol. **31**, 035013 (2020).
11. G. Mueller, Q.-z. Shu, R. Adhikari, *et al.*, "Determination and optimization of mode matching into optical cavities by heterodyne detection," Opt. Lett. **25**, 266 (2000).
12. A. Stochino, K. Arai, and R. X. Adhikari, "Technique for in situ measurement of free spectral range and transverse mode spacing of optical cavities," Appl. Opt. **51**, 6571 (2012).
13. K. M. Manfred, L. Ciaffoni, and G. A. D. Ritchie, "Optical-feedback cavity-enhanced absorption spectroscopy in a linear cavity: model and experiments," Appl. Phys. B **120**, 329–339 (2015).
14. M. Rakhmanov, F. Bondu, O. Debieu, and R. L. Savage, "Characterization of the LIGO 4 km Fabry–Perot cavities via their high-frequency dynamic responses to length and laser frequency variations," Class. Quantum Gravity **21**, S487–S492 (2004).
15. M. Casado, T. Stoltmann, A. Landais, *et al.*, "High stability in near-infrared spectroscopy: part 1, adapting clock techniques to optical feedback," Appl. Phys. B **128**, 54 (2022).
16. J. Morville, S. Kassi, M. Chenevier, and D. Romanini, "Fast, low-noise, mode-by-mode, cavity-enhanced absorption spectroscopy by diode-laser self-locking," Appl. Phys. B **80**, 1027–1038 (2005).
17. E. Kerstel, R. Iannone, M. Chenevier, *et al.*, "A water isotope (2H, 17O, and 18O) spectrometer based on optical feedback cavity-enhanced absorption for in situ airborne applications," Appl. Phys. B **85**, 397–406 (2006).
18. K. K. Lehmann and D. Romanini, "The superposition principle and cavity ring-down spectroscopy," The J. Chem. Phys. **105**, 10263–10277 (1996).
19. A. Yariv, *Quantum Electronics* (John Wiley & Sons, California Insitutute of Technology, 1989), 3rd ed.
20. D. Romanini, "Modelling the excitation field of an optical resonator," Appl. Phys. B **115**, 517–531 (2014).
21. J. A. Arnaud and H. Kogelnik, "Gaussian Light Beams with General Astigmatism," Appl. Opt. **8**, 1687 (1969).